Influence of Boron Content on Glass Forming Ability and Soft Magnetic Properties in Fe-Si-B-Nb-Cu Nanocrystalline Alloys for Gas Atomization

Subong An^{1,2}, Hyun Ah Im^{1,2}, Nguyen Thi Thanh Na¹, Kyeong-mi Jang¹, Jung Woo Lee^{2*}, and Jae Won Jeong^{1*}

¹Metal Powder Department, Korea Institute of Materials Science (KIMS), 797 Changwondae-ro, Seongsan-gu,
Changwon 51508, Republic of Korea

²School of Materials Science and Engineering, Pusan National University, Busandaehak-ro 63beon-gil, Geumjeong-gu,
Busan 46241, Republic of Korea

(Received 19 June 2025, Received in final form 1 July 2025, Accepted 1 July 2025)

In this study, we investigated the effects of boron addition on glass forming ability (GFA) and soft magnetic properties of $Fe_{73.5}Si_{13.5-x}B_{9+x}Nb_3Cu_1$ nanocrystalline alloys. By increasing the boron content in the alloys, GFA is expected to be increased via calculation on thermodynamic factors including mixing enthalpy, mixing entropy, and atomic radius differences. This enhancement in GFA is highly beneficial for powder production via gas atomization. Since gas atomization typically exhibits a lower cooling rate compared to the melt spinning process, achieving an amorphous structure is more challenging. However, by improving the GFA through alloy design, amorphous phase formation was successfully demonstrated even under these conditions. As a result, it was confirmed that the fully amorphous powders exhibited significantly improved coercivity compared to powders with initial crystallites. This alloy-design-based approach not only contributes to cost reduction in processing by enabling amorphous formation under less stringent cooling conditions, but also leads to enhanced magnetic properties.

Keywords: soft magnetic materials, nanocrystalline alloy, gas atomization, soft magnetic properties, glass forming ability

1. Introduction

Soft magnetic materials are widely utilized in various applications due to their excellent magnetic properties. These materials are processed into different forms such as ribbons, sheets, and powders [1–3]. In particular, powder-type soft magnetic materials offer the advantage of easy shape control through compression molding techniques [4]. Thanks to these benefits, soft magnetic powders have become highly desirable for use in electrical devices and components, including inductors [5, 6]. With the ongoing trend toward miniaturization and improved efficiency in electronic components, the demand for advanced

materials is increasing [7]. In this context, nanocrystalline soft magnetic powders are especially promising, as they exhibit superior magnetic performance compared to conventional soft magnetic materials [8]. These materials typically consist of nanograins approximately 20 nm in size embedded in an amorphous matrix [9].

This unique structure contributes to excellent magnetic characteristics, such as low coercivity and high permeability [10]. The presence of numerous nanocrystals enables enhanced magnetic properties through exchange interactions between neighboring grains, which helps reduce magnetic anisotropy [11]. Soft magnetic powder is typically fabricated by gas atomization process which includes melting the alloy and spraying the molten alloy with high pressure gas [12]. As a result, the amorphous and sphere-shape powder can be produced. The process makes more easily the alloy with high GFA, but the fabrication of the nanocrystalline powders consisting of copper (Cu) is difficult. Because the Cu has a positive mixing enthalpy with Fe, thereby overall mixing enthalpy

©The Korean Magnetics Society. All rights reserved.

*Corresponding author: Dr. Jae Won Jeong

E-mail: jeongjw1204@kims.re.kr

Tel: +82-55-280-3611 Prof. Jung Woo Lee

E-mail: jungwoolee@pusan.ac.kr

of alloy increases. Moreover, Cu tends to form fine nano clusters in the amorphous matrix, which inhibits the formation of fully amorphous state, it leads to decrease the GFA [13]. As a result, when the cooling rate provided by the gas atomization process is insufficient to fully suppress crystallization, the formation of a completely amorphous structure becomes challenging, particularly for nanocrystalline-type compositions [14, 15]. This often leads to the occurrence of powders containing partial crystalline phases. Also, after heat treatment to such powders, it may lead to significant grain coarsening due to the presence of pre-existing crystalline phases, thereby deteriorating the magnetic properties [16].

To solve the problem, it needs to enhance the cooling rate in atomization process. However, equipment upgrades or process modifications increases production complexity and cost. Alternatively, the designing new alloy composition to enhance the GFA can be more economical and effective way. Such compositional design can minimize the reliance on advanced processing technologies while enabling the fabrication of high-quality amorphous or nanocrystalline powders with desirable properties.

In this study, we aimed to enhance the GFA by modifying the composition of FINEMET [17] (Fe_{73.5}Si_{13.5}B₉Nb₃Cu₁), a representative nanocrystalline soft magnetic alloy, through the reduction of silicon (Si) content and the corresponding increase in boron (B) content. B is known to improve the GFA of Fe-based soft magnetic alloys due to its small atomic radius and large negative mixing enthalpy with Fe and other constituent elements [18, 19]. Therefore, increasing the B content is expected to be effective in enhancing the GFA [20]. To evaluate the improvement in GFA, ribbons were fabricated using the melt spinning method. By varying the wheel speed, different cooling rates were simulated, the GFA of the designed alloys ribbons was compared. After optimizing the composition of alloy, we confirmed whether the alloy could also retain an amorphous state when processed by gas atomization. As a result, the newly designed alloy with increased boron content showed a more distinct formation of a fully amorphous phase, confirming the enhancement of GFA in the modified composition. Based on this optimized composition, fully amorphous nanocrystalline powders were successfully fabricated via the gas atomization process, and their structural and magnetic properties were evaluated. The optimized powders exhibited significantly improved magnetic properties compared to the original composition, validating the effectiveness of the alloy design strategy proposed in this study.

2. Experimental

2.1. Materials

The following materials were purchased from TAEWON SCIENTIFIC CO., Korea: Fe (99.95 wt.%), Si (99.999 wt.%), Cu (99.997 wt.%), Fe-B (mixed 85/15 wt.%, 99.9 wt.%), Fe-Nb (mixed 50:50 at.%, 99.5 wt.%). The quartz tube, with an outer diameter of 15 mm, an inner diameter of 12 mm, and a length of 150 mm, along with a rectangular slit measuring 0.2 mm by 5 mm, was purchased from Y&I Tech CO., Korea.

2.2. Fabrication of the alloys

The $Fe_{73.5}Si_{13.5-x}B_{9+x}Nb_3Cu_1$ alloys for melt spinning were fabricated using an arc melting method. The alloy ingots were weighed to 10.000 g, with precision to three decimal places. The specific compositions of the alloys, designated as FINEMET, #1, #2, and #3, are detailed in Table 1. The alloys were produced in a high-purity argon (Ar, 99.999%) atmosphere to prevent oxidation, following high vacuum atmosphere of 10^{-4} Pa. To ensure thorough mixing, the alloy was flipped back and 4 to 5 times to produce the final ingot.

2.3. Fabrication of the powder and ribbons

The $Fe_{73.5}Si_{13.5-x}B_{9+x}Nb_3Cu_1$ powder and ribbons were fabricated by gas atomization and melt spinning. The powder was supplied from ZENIX Co., Korea and the ribbons were produced under different wheel speed conditions, with a copper wheel speed of 5 to 30 m/s, an injection pressure of 20 kPa, and a distance of 0.1 mm between the wheel and the nozzle. Fabricated ribbons measured 5 mm in width and 20 μ m in thickness.

2.4. Nanocrystallization of powder and ribbons

To compare on amorphous and nanocrystalline powder, we treated the annealing process in muffle furnace in Ar atmosphere. We conducted annealing from 525, 550, 580 °C to obtain proper temperature for nanocrystalline matrix. The nanocrystallization was analyzed by XRD.

Table 1. The precise compositions of $Fe_{73.5}Si_{13.5-x}B_{9+x}Nb_3Cu_1$ alloys.

Alloy	$Fe_{73.5}Si_{13.5-x}B_{9+x}Nb_3Cu_1$
FINEMET	$Fe_{73.5}Si_{13.5}B_9Nb_3Cu_1$
#1	$Fe_{73.5}Si_{12.5}B_{10}Nb_3Cu_1$
#2	$Fe_{73.5}Si_{11.5}B_{11}Nb_3Cu_1$
#3	$Fe_{73.5}Si_{10.5}B_{12}Nb_3Cu_1$

2.5. Characterization

The structures of the amorphous and nanocrystalline powder was analyzed via X-ray diffraction (XRD; Rigaku D/Max-2500VL/PC). The magnetic properties of powder were analyzed by DC loop tracer (Remagraph C-500, MAGNET-PHYSIK) under an applied field of 800 A/m, and the vibrating sample magnetometer (VSM; EZ9, Microsense) under an applied magnetic field of 15000 Oe. And the microstructure of sample was confirmed by using field emission transmission electron microscopy (FE-TEM; Talos F200X, Thermo Fisher Scientific).

3. Results and Discussions

Figure 1 presents the strategies of developing nanocrystalline soft magnetic powders with compositions of $Fe_{73.5}Si_{13.5-x}B_{9+x}Nb_3Cu_1$ to enhance GFA and magnetic properties by designing the alloy composition. The soft magnetic powder was produced by using gas atomization that has 10^2-10^4 K/s cooling rates [21], that process

illustrated in Fig. 1a. From gas atomization process, some powder fabricated with amorphous and crystals phases in the initial state result from low cooling rate of gas atomization. In the Fig. 1b, there are two kinds of alloy consist of high and low GFA alloy that are formed fully amorphous and with crystals and amorphous dual phases. The initial structural characterization can be obtained from XRD result, in the Fig. 1c. When the alloy of low GFA composition was fabricated, the alloy has the crystal peaks in (110) and (200) plane of α -Fe at $2\theta = 45^{\circ}$ and 65°. Otherwise, the alloy of high GFA composition has the amorphous phase without any crystal peaks. When the annealing to alloy for nanocrystallization, the alloy has crystal peaks in the initial state, the crystals in the matrix could be have abnormal grain growth. It can be led to deteriorate the magnetic properties [22, 23]. Because the uneven grains lead to interrupt to exchange interactions [24]. Therefore, the initial structure of alloy fabricated gas atomization has to be fully amorphous phases for enhancing magnetic properties. To obtain fully amorph-

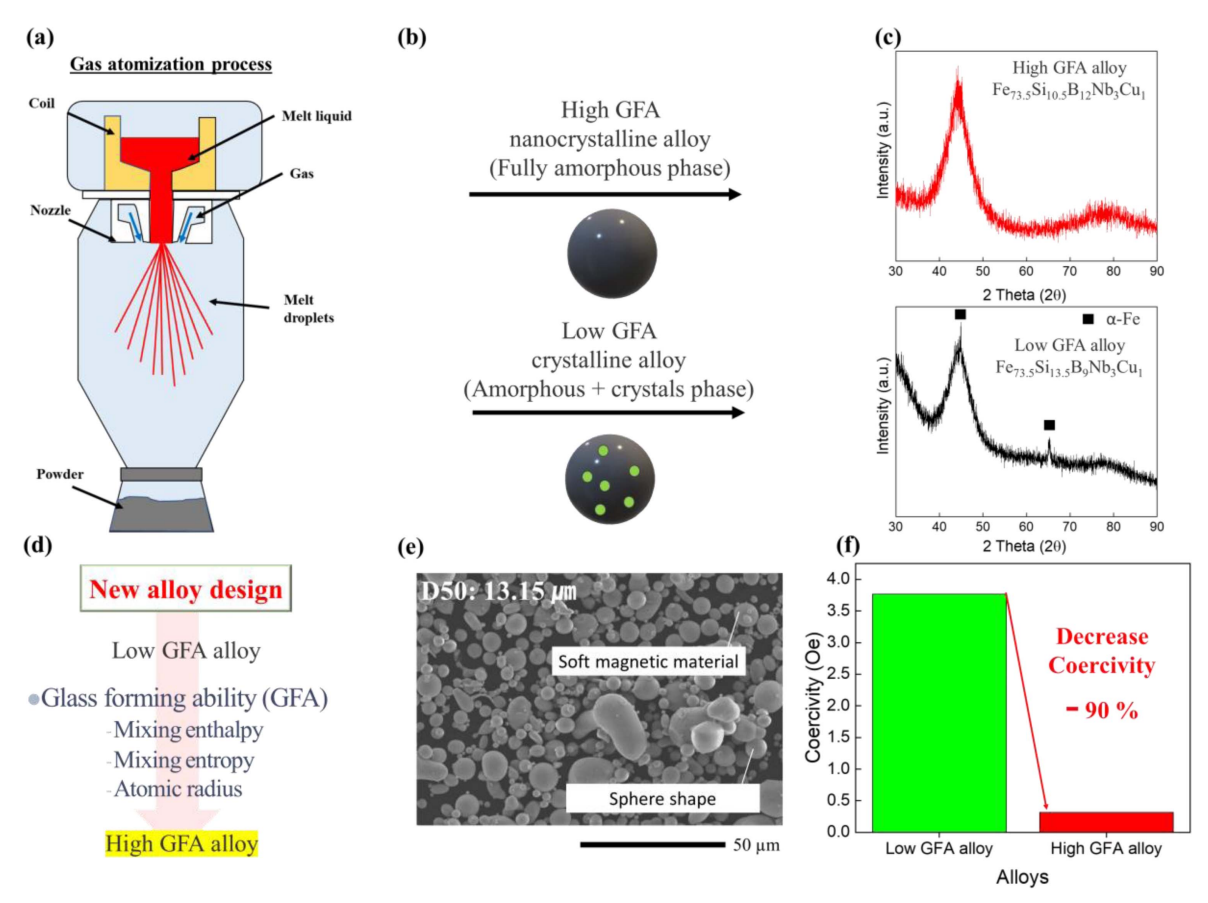


Fig. 1. (Color online) Manufacturing overview of nanocrystalline soft magnetic sphere shape powder with low coercivity performance. (a) Schematic illustration showing the gas atomization for fabricating sphere shape metal powder. (b, c) Comparison of (b) phase different and (c) structural characterization on high and low GFA powder. (d) Strategy on designing new alloy with several GFA factors. (e) SEM image of Fe_{73.5}Si_{10.5}B₁₂Nb₃Cu₁ powder. (f) Coercivity data of low and high GFA alloy.

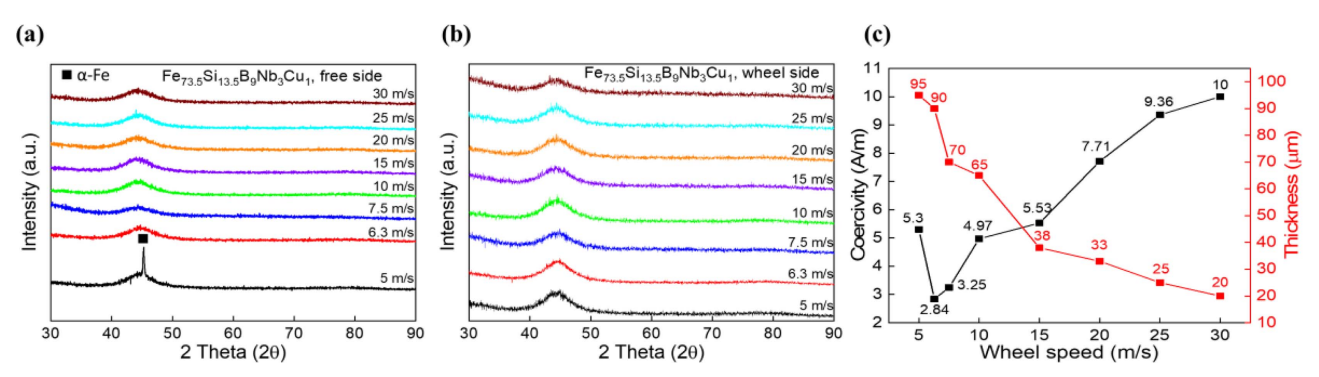


Fig. 2. (Color online) (a, b) XRD data of Fe_{73.5}Si_{13.5}B₉Nb₃Cu₁ ribbons with (a) free side and (b) wheel side. (c) The comparison of coercivity and thickness of each ribbon were fabricated on several wheel speed conditions utilized melt spinning.

ous powder, we set the strategy by designing new alloy with calculation of GFA factors, as mixing enthalpy, mixing entropy, and atomic radius differences. It can be seen in Fig. 1d. In the Fig. 1e, the SEM result of soft magnetic powder of sphere shape presented with D50 of 13.15 µm. The Fig. 1f shows the enhanced coercivity as magnetic properties between annealed low GFA alloy and high GFA alloy. High GFA alloy have low coercivity compared the low GFA alloy around decreased 90 %. Based on the results, the initial phase of powder is important for properties. In other words, despite the inherent difficulty of producing fully amorphous powders through the gas atomization process, the designing of alloy enabled the successful fabrication of fully amorphous powders. As a result, the magnetic properties were improved compared to conventional powders with partial crystallinity. The following figure will explain the alloy design strategy and the experimental approach employed to achieve high GFA.

Figure 2 shows the structural and magnetic characterization of Fe_{73.5}Si_{13.5}B₉Nb₃Cu₁ ribbons. When the conventional FINEMET alloy was processed via gas atomization, fully amorphous powders could not be obtained; instead, partially crystalline powders were produced. To address this issue, we aimed to develop a new alloy composition capable of forming a fully amorphous phase. As a first step, ribbons were fabricated from the conventional FINEMET alloy using the melt spinning process. The wheel speed, which directly affects the cooling rate, was gradually reduced from 30 m/s to 5 m/s in order to identify the condition at which crystallization begins. Based on this identified condition, further experiments were conducted using the newly designed alloy to determine whether it could maintain an amorphous structure under the same low cooling rate. Fig. 2a and b shows the XRD results of free side and wheel side of Fe_{73.5}Si_{13.5}B₉Nb₃Cu₁ ribbons under

fabricated 30 m/s - 5 m/s separately. Since the wheel side is in direct contact with the copper wheel, it exhibits a higher cooling rate than the free side [25]. Therefore, XRD analysis was performed on both sides to compare their structural differences. Based on the results from both sides of the ribbon, a crystal peak corresponding to the (110) plane of α -Fe at $2\theta = 45^{\circ}$ was confirmed on the free side at a wheel speed of 5 m/s. This observation indicates that at a cooling rate corresponding to 5 m/s, the alloy fails to form a fully amorphous structure on FINEMET. Fig. 2c compares the thickness and coercivity of the fabricated ribbons. As the wheel speed decreases, the ribbon thickness gradually increases. The coercivity tends to decrease with increasing ribbon thickness. However, a subsequent increase in coercivity was observed in samples exhibiting crystalline phases. This suggests a degradation in magnetic properties due to crystallization. The decrease in coercivity with increasing ribbon thickness is attributed to the pinning effect arising from surface defects, which can enhance the effective packing density of magnetic domains [26]. Based on these results, it was confirmed that the conventional FINEMET alloy exhibits crystalline phases when processed at a wheel speed of 5 m/s. To improve the GFA, a new alloy composition with increased B content was designed and fabricated into ribbons using melt spinning at the same wheel speed of 5 m/s. If the resulting ribbon maintains a fully amorphous structure under this condition, it indicates that the GFA of the newly designed alloy has been successfully enhanced.

Figure 3 and Table 2 shows the thermodynamic parameters related to the GFA of $Fe_{73.5}Si_{13.5-x}B_{9+x}Nb_3Cu_1$ alloys. Based on these calculations, the effect of compositional variations on GFA was theoretically evaluated in this study. The alloys were designed by decreasing 1 at% of Si and increasing 1 at% of B for enhancing GFA. The results of GFA can be calculated by

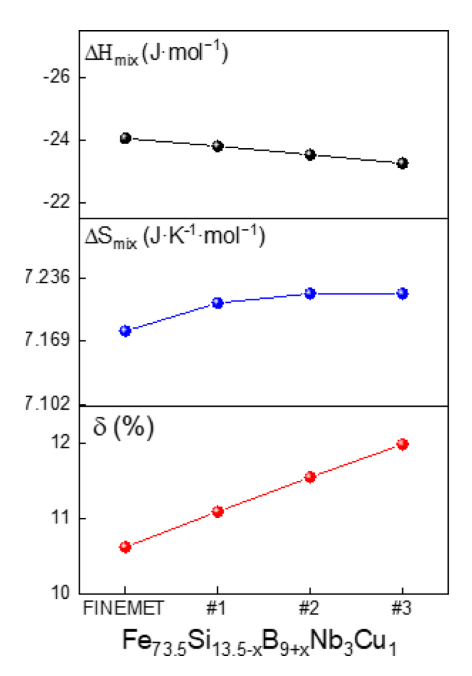


Fig. 3. (Color online) Comparison of mixing enthalpy (ΔH_{mix}), mixing entropy (ΔS_{mix}), and atomic size difference (δ) of the $Fe_{73.5}Si_{13.5-x}B_{9+x}Nb_3Cu_1$ alloy with varying boron content.

Table 2. Comparison of mixing enthalpy (ΔH_{mix}) , mixing entropy (ΔS_{mix}) , and atomic size difference (δ) of the $Fe_{73.5}Si_{13.5-x}B_{9+x}Nb_3Cu_1$ alloys.

	· ·		
Alloy	ΔH_{mix} $(J \cdot mol^{-1})$	ΔS_{mix} $(J \cdot K^{-1} \cdot mol^{-1})$	δ (%)
FINEMET	- 24.07	7.18	10.61
#1	- 23.85	7.21	11.09
#2	- 23.55	7.22	11.55
#3	- 23.27	7.22	12.00

mixing enthalpy, mixing entropy, and atomic radius difference. The mixing enthalpy [18, 19], ΔH_{mix} , is defined as:

$$\Delta H_{\text{mix}} = \sum_{i=1, i \neq i}^{n} 4\Delta H_{mix}^{AB} c_i c_i \tag{1}$$

 $\Delta H_{\rm mix}^{AB}$ is the mixing enthalpy between A and B elements and c_ic_j are atomic percent. It is well known that a larger negative value of the mixing enthalpy enhances the GFA of an alloy by stabilizing the formation of the amorphous phase. As a result, the mixing enthalpy was found to increase from -24.07 kJ/mol to -23.27 kJ/mol by increasing B content in alloy, corresponding to an increase of approximately 3.3%. This change can be explained by considering that the mixing enthalpy between Fe and Si is approximately -35 kJ/mol, while that between Fe and B is around -26 kJ/mol. Although a slight increase in mixing enthalpy was observed, the 3.3% increase is relatively minor and is not expected to cause a significant difference in the GFA of the alloy. Also, the mixing entropy [26], $\Delta S_{\rm mix}$, is defined as :

$$\Delta S_{mix} = -R \sum_{i=1}^{n} c_i ln c_i$$
 (2)

R is the gas constant. The mixing entropy reflects the degree of atomic mixing and indicates the overall compositional randomness of the alloy. In the present results, no significant difference was observed in the mixing entropy. In contrast, the atomic radius differences exhibited a noticeable variation. The atomic radius differences [27], δ , is defined as:

$$\delta = 100\sqrt{\sum_{i=1}^{n} c_i (1 - r_i/\bar{r})^2}$$
 (3)

 \overline{r} is the average atomic radius. A large atomic radius

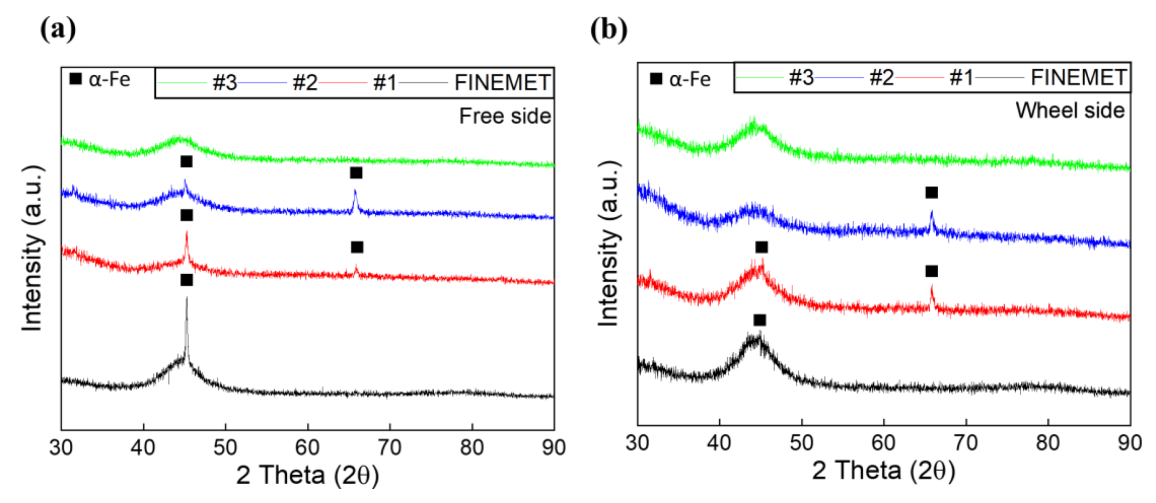


Fig. 4. (Color online) (a, b) XRD data of Fe_{73.5}Si_{13.5-x}B_{9+x}Nb₃Cu₁ ribbons with (a) free side and (b) wheel side.

difference hinders atomic diffusion, thereby promoting denser atomic packing, which is known to enhance the GFA. Also, according to the amorphous formation rule [20], an atomic radius difference of over 12% or more facilitates the formation of an amorphous phase. As a result, it was confirmed that the atomic radius difference increased by approximately 13% with increasing B content. This can be attributed to the significant

difference in atomic radius between Si (0.1153 nm) and B (0.082 nm). Based on this, alloy #3 is expected to exhibit the highest GFA among the investigated compositions. This calculation approach is expected to provide a more accessible method for identifying alloys with high GFA [28].

Figure 4 shows the structural properties with XRD results of $Fe_{73.5}Si_{13.5-x}B_{9+x}Nb_3Cu_1$ ribbons with free side

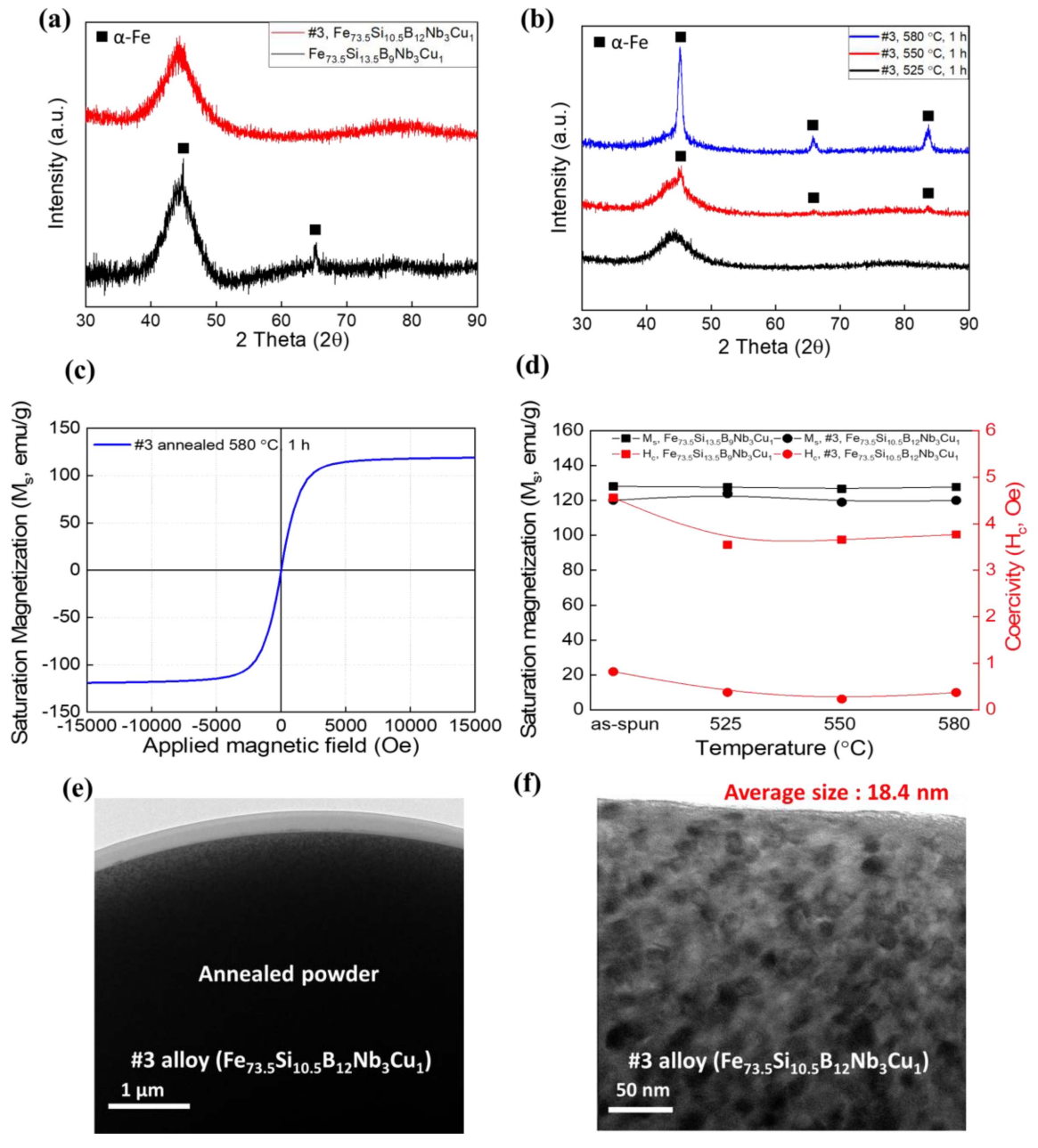


Fig. 5. (Color online) Structural and magnetic characterization of both amorphous and nanocrystalline powder. (a, b) XRD data of $Fe_{73.5}Si_{13.5}B_9Nb_3Cu_1$ and #3 alloy $(Fe_{73.5}Si_{10.5}B_{12}Nb_3Cu_1)$ powder on different conditions of (a) as-cast and (b) annealed at 525, 550, and 580 °C in 1 h. (c) VSM plot of #3 alloy $(Fe_{73.5}Si_{10.5}B_{12}Nb_3Cu_1)$ annealed powder. (d) Comparison of saturation magnetization (black color) and coercivity (red color) of $Fe_{73.5}Si_{13.5}B_9Nb_3Cu_1$ and #3 alloy $(Fe_{73.5}Si_{10.5}B_{12}Nb_3Cu_1)$ powder. (e,f) TEM images of #3 alloy $(Fe_{73.5}Si_{10.5}B_{12}Nb_3Cu_1)$ nanocrystalline powder annealed at 580 °C in 1 h.

(a) and wheel side (b). All ribbons were fabricated at a wheel speed of 5 m/s, which corresponds to the critical condition that does not satisfy the cooling rate required for amorphous formation for FINEMET alloy, as shown in Fig. 2. As a result, distinct crystalline peaks corresponding to the (110) and (200) planes of α-Fe at $2\theta = 45^{\circ}$ and 65° , respectively, were observed in all alloy ribbons except for alloy #3. These results are consistent with the trends predicted by the calculated GFA-related factors, supporting the expectation that alloy #3 possesses the highest GFA among the tested compositions. Through ribbon-based experiments, the improvement in GFA achieved via alloy design was confirmed. As a result, alloy #3, which contained an additional 3 at% of B, exhibited the highest GFA. Based on this finding, spherical powders were subsequently produced using gas atomization, and their structural and magnetic properties were comparatively analyzed.

Figure 5 shows the structural and magnetic characterization of amorphous and nanocrystalline powder. Fig. 5a shows the XRD results of initial state of powders with composition of Fe_{73.5}Si_{13.5}B₉Nb₃Cu₁ and #3 alloy prepared by gas atomization. As a result, the XRD pattern of alloy #3, which was expected to exhibit the high GFA, confirmed the formation of a fully amorphous phase. This indicates that the addition of B effectively enhanced the GFA. Consequently, even in the powder fabricated via gas atomization, the improved GFA was clearly demonstrated. To induce nanocrystallization in alloy #3, heat treatments were performed at 525 °C, 550 °C, and 580 °C for 1 hour in a muffle furnace under an argon atmosphere. XRD analysis was conducted to evaluate the extent of nanocrystallization, and the results are presented in Fig. 5b. In the sample annealed at 580 °C, distinct crystallization peaks corresponding to the (110), (200), and (211) planes were observed at $2\theta = 45^{\circ}$, 65° , and 82° , respectively. These results indicate that crystallization was successfully achieved at this temperature. Subsequently, Fe_{73 5}Si_{13 5}B₉Nb₃Cu₁ powder was also subjected to nanocrystallization under the same heat treatment conditions, and the magnetic properties of the nanocrystallized powders were compared. The results can be seen in Fig. 5c and d, and Table 3. As a result, the saturation magnetization (M_s) measured by VSM was found to be slightly lower in alloy #3. The Si content was reduced and B was increased in alloy #3, the saturation magnetization decreased. B is a paramagnetic element that dilutes the ferromagnetic moment of iron, resulting in a slight decrease in the M_s [29]. Also, the FINEMET alloy exhibits a relatively high M_s value due to partial crystallization at the initial stage from XRD result. Furthermore,

Table 3. Comparison of saturation magnetization and coercivity of $Fe_{73.5}Si_{13.5}B_9Nb_3Cu_1$ and #3 ($Fe_{73.5}Si_{10.5}B_{12}Nb_3Cu_1$) powder.

Alloy	Annealing temperature, 1 h					
	Properties	as-spun	525 °C	550 °C	580 °C	
FINEMET	M _s (emu/g)	128.05	127.76	126.67	127.74	
	H _c (Oe)	4.56	3.55	3.66	3.77	
#3	M _s (emu/g)	120.12	125.28	123.91	119.01	
	H _c (Oe)	0.82	0.509	0.34	0.23	

thermal annealing promotes the formation of high-density α-Fe nanocrystals, which contributes to a further increase in M_s. However, the difference between the pre-existing crystallites and those formed during annealing appears to weaken the exchange interaction between grains, thereby leading to an increase in coercivity [11, 30, 31]. However, when comparing the samples annealed at 580 °C, the decrease in saturation magnetization was only about 5.5%, while a significant improvement in coercivity was observed. The coercivity of the partially crystallized powder was 3.77 Oe, whereas that of the well-amorphized #3 alloy was reduced to 0.23 Oe, representing approximately a 90% decrease. This suggests that, compared to alloys that had already undergone initial crystallization, the #3 alloy maintained its amorphous state more effectively and, upon annealing, formed uniformly distributed nanocrystals. TEM observations were conducted to investigate the nanocrystallization behavior, as shown in Fig. 5e and f. Fig. 5e presents the TEM images of the annealed powder fabricated from the #3 alloy using a gas atomizer. Fig. 5f shows a high magnification image of the annealed powder. The average grain size was measured to be approximately 18.4 nm, and the nanocrystals were densely distributed within the amorphous matrix. As a result, enhanced exchange interactions between the nanocrystals led to superior magnetic properties [11]. In summary, the results confirmed that compositional modification is effective for improving GFA and magnetic properties of Fe-based nanocrystalline soft magnetic powders.

4. Conclusion

In this study, we demonstrated that the GFA of Febased soft magnetic nanocrystalline alloys can be effectively enhanced by increasing the B content. The designed alloy, Fe_{73.5}Si_{10.5}B₁₂Nb₃Cu₁, successfully formed a fully amorphous structure even under the gas atomization. The enhancement in GFA was initially

predicted using thermodynamic factor calculations and subsequently verified through melt spinning experiments and XRD analysis. As a result, the optimized alloy exhibited significantly reduced coercivity after nanocrystallization, highlighting the advantages of starting from a fully amorphous state. These findings suggest that composition-based GFA optimization is a practical and effective approach for developing high-performance soft magnetic powders using gas atomization.

Data availability

Data will be made available on request.

Declaration of Competing Interest

The authors declare that they have no known competing financial interests or personal relationships that could have appeared to influence the work reported in this paper.

Acknowledgements

This work was supported by Material and Component Technology Development Project funded by the Korea Ministry of Trade, Industry and Energy (MOTIE, Korea), and Korea Institute of Materials Science [Project number: 20026708 and PNKA510].

References

- [1] G. E. Fish, Proceedings of the IEEE 78, 947 (2002).
- [2] F. Fiorillo, G. Bertotti, C. Appino, and M. Pasquale, Wiley Encyclopedia of Electrical and Electronics Engineering, 1 (2016).
- [3] J. M. Silveyra, E. Ferrara, D. L. Huber, and T. C. Monson, Science. **362**, eaao0195 (2018).
- [4] V. Boljanovic, Metal shaping processes: casting and molding, particulate processing, deformation processes, and metal removal, Industrial Press Inc., South Norwalk (2010) pp. 3-5.
- [5] J.-G. Yeo, D. H. Kim, Y. J. Choi, and B. W. Lee, J. Electron. Mater. 48, 6018 (2019).
- [6] B. S. Ram, A. Paul, and S. Kulkarni, J. Magn. Magn. Mater. 537, 168210 (2021).
- [7] X. Lin and M. Han, Soft Science 3, 14 (2023)
- [8] A. Yakin, T. Simsek, B. Avar, T. Simsek, and A. K. Chattopadhyay, Emerg. Mater. 6, 453 (2023).

- [9] Y. Liu, Y. Yi, W. Shao, and Y. Shao, J. Magn. Magn. Mater. 330, 119 (2013).
- [10] K. Lv, Y. Li, N. Shen, G. Li, Y. Wang, and X. Hui, J. Non-Cryst. Solids. 578, 121355 (2022).
- [11] G. Herzer, Acta Mater. 61, 718 (2013).
- [12] K. L. Alvarez, J. M. Martín, M. Ipatov, and J. Gonzalez, J. Alloys Compd. 735, 2646 (2018)
- [13] H. Li, J. Gao, Y. Wu, Z. Jiao, D. Ma, A. Stoica, X. Wang, Y. Ren, M. Miller, and Z. Lu, Sci. Rep. 3, 1983 (2013).
- [14] Y. Shi, W. Lu, W. Sun, S. Zhang, B. Yang, and J. Wang, J. Alloys. Compd. 920, 166038 (2022).
- [15] G. Li, G. Shi, H. Miao, D. Liu, Z. Li, M. Wang, and L. Wang, Mater. 16, 1284 (2023).
- [16] Z. Chen, S. Kang, Q. Zhu, K. Zhang, J. Hu, and Y. Jiang, J. Alloys Compd. 968, 172116 (2023).
- [17] Y. A. Yoshizawa, S. Oguma, and K. Yamauchi, J. Appl. Phys. 64, 6044 (1988).
- [18] A. Takeuchi and A. Inoue, Mater. Trans. 46, 2817 (2005).
- [19] A. Takeuchi and A. Inoue, Mater. Trans. 41, 1372 (2000).
- [20] A. Inoue, Acta Mater. 48, 279 (2000).
- [21] T. Zhao, C. Chen, X. Wu, C. Zhang, A. A. Volinsky, and J. Hao, J. Alloys Compd. 857, 157991 (2021).
- [22] M. Ohta and Y. Yoshizawa, Jpn. J. Appl. Phys. **46**, L477 (2007)
- [23] E. Lopatina, I. Soldatov, V. Budinsky, M. Marsilius, L. Schultz, G. Herzer, and R. Schäfer, Acta Mater. 96, 10 (2015).
- [24] G. Herzer, Phys. Scr. 1993, 307 (1993).
- [25] L. Abadlia, M. I. Daoudi, and S. Alleg, Appl. Phys. A. **129**, 487 (2023).
- [26] M.-C. Lee, C.-Y. Lin, S.-H. Wang, and T.-S. Chin, IEEE Trans. Magn. **44**, 3836 (2008).
- [27] R. Feng, M.C. Gao, C. Lee, M. Mathes, T. Zuo, S. Chen, J. A. Hawk, Y. Zhang, and P. K. Liaw, Entropy 18, 333 (2016).
- [28] S. Fang, X. Xiao, L. Xia, W. Li, and Y. Dong, J. Non-Cryst. Solids. 321, 120 (2003).
- [29] O. Senkov and D. Miracle, Mater. Res. Bull. **36**, 2183 (2001).
- [30] G. Ouyang, R. Claude, A. Kovar, B. Hillard, M. J. Kramer, I. E. Anderson, and J. Cui, JOM 76, 1044 (2024).
- [31] H. Yi, H. Li, S. Zhang, C. Chen, R. Wei, S. Wu, Y. Cai, F. Li, and T. Wang, J. Mater. Eng. Perform. 1 (2024).
- [32] Y. Fan, S. Zhang, X. Xu, J. Miao, W. Zhang, T. Wang, C. Chen, R. Wei, and F. Li, Intermetallics 138, 107306 (2021).